American Mineralogist, Volume 69, pages 788–799, 1984

The electronic structures of manganese oxide minerals

DAVID M. SHERMAN

Department of Earth and Planetary Sciences
Massachusetts Institute of Technology
Cambridge, Massachusetts 02139

Abstract

Molecular orbital calculations, using the Xα scattered wave method, were done for the clusters MnO_6^{10-}, MnO_6^{9-}, and MnO_6^{8-} corresponding to Mn^{2+}, Mn^{3+}, and Mn^{4+} in octahedral coordination with O^{2-}. Bond lengths representative of those observed in manganese oxides were chosen and O_h symmetry was used for each cluster.

The calculated orbital energies and charge distributions are used to describe the nature of chemical bonding in manganese oxides. Spectroscopic transition energies are calculated and these are compared with experimental optical, X-ray emission and photoelectron (ESCA) spectra of manganese oxides. The agreement between the calculated and experimental spectroscopic transition energies is fairly good and indicates that isolated clusters can be used to model the localized aspects of the electronic structure of manganese oxide minerals.

The electronic structure of these clusters can also be related to the crystal chemistry of the manganese oxides. In spite of radius ratio considerations, Mn^{4+} is found to be considerably more stable in octahedral rather than tetrahedral coordination. This is demonstrated by comparing the electronic structure of MnO_6^{8-} with that of a tetrahedral MnO_4^{4-} cluster. A large degree of covalency in the MnO_6^{8-} cluster is consistent with the strong Lewis acidity of Mn^{4+}. In contrast, the bonding in MnO_6^{10-} is mostly ionic. The calculated exchange splittings of the crystal field orbitals show that low-spin Mn^{2+} should not exist even under high-pressure, but that low spin Mn^{3+} may substitute for Mn^{4+} in manganese (IV) oxides.

Introduction

In natural environments manganese occurs in the Mn(II), Mn(III) and Mn(IV) oxidation states. All three valences form a large number of oxide minerals, ranging from the simple phases manganosite (MnO), partridgite (Mn_2O_3) and pyrolusite (MnO_2) to complex mixed-valence oxides such as birnessite ($(Ca,Na)(Mn^{2+},Mn^{4+})_7O_{14} \cdot 3H_2O$) and todorokite ($(Na,Ca,K,Ba,Mn^{2+})_2Mn_5O_{12} \cdot 3H_2O$) (see, for example, Burns and Burns, 1977, 1979).

The classical ionic bonding model of Pauling, although often useful, cannot rationalize all of the observed trends in the crystal chemistry of these minerals. Many of the physical properties, crystal-chemical trends and consequent geochemical behavior of manganese oxides can only be understood in the context of quantum chemistry. In this regard, the partially occupied Mn 3*d* orbitals, the existence of more than one formal oxidation state of manganese, and the diverse types of Mn–O and Mn–Mn interactions give rise to a number of theoretical problems not associated with other minerals. On a more practical side, a number of electronic spectroscopic techniques are of direct mineralogical application to the determination of cation valence states and coordination environments in manganese oxides and, in particular, the complex and poorly crystalline phases in marine manganese oxide nodules. Such electronic spectra are difficult to interpret, however, without a theoretical understanding of the nature and approximate relative energies of the electronic states being investigated. In short, a greater understanding of the crystal chemistry, physical properties and electronic spectra of manganese oxides requires an understanding of their electronic structures.

A complete description of the electronic structure of a mineral can only be achieved using band theory. However, the accurate calculation of electronic energy bands in solids with more than a few atoms per unit cell is often infeasible. In theory, the electronic states of a mineral must be invariant under the operations of its crystallographic space group. In practice, one often finds that the electronic structure of a system is only weakly dependent upon the translational periodicity of the atomic arrangements. This follows because electrons in solids are generally localized to small atomic regions. This localized nature of electrons suggests an alternative, albeit less

0003–004X/84/0708–0788$02.00

rigorous, approach to investigating the electronic structure of minerals. Following Tossell and Gibbs (1977), it shall be referred to as the cluster molecular orbital method (for a detailed discussion, see Slater, 1974). Here, the electronic structure of a solid is approximated by that of a finite cluster of atoms. For example, the electronic structure of MnO might be approximated by that of an octahedral MnO_6^{10-} cluster. Ideally, the atomic cluster is large enough to accommodate most of the spatial dimensions over which an electron is delocalized in the solid. In general, as the atomic cluster becomes infinitely large, its electronic structure will converge to that of the solid. However, if the electrons in the solid are fairly localized, then this convergence limit might be approximately achieved by the electronic structure of a small cluster of atoms.

There are a large number of molecular orbital methods with which one may calculate the approximate electronic structure of atomic clusters. Of these, the Xα-Scattered Wave method (described below) is the most useful for clusters and molecules containing transition metals. The cluster molecular orbital approach, using the Xα-scattered wave method, has been applied to several transition metal oxides. For example, Tossell et al. (1974) investigated the electronic structure of iron and titanium oxides using molecular orbital calculations on FeO_6^{10-}, FeO_6^{9-} and TiO_6^{8-}. The close agreement between the calculated molecular orbital energies and the experimental spectra of iron and titanium oxides demonstrate that the cluster approach can provide a good approximation to the electronic structure of minerals.

In the crystal structures of the manganese oxides, manganese cations are octahedrally coordinated by oxygen anions; the resulting MnO_6 polyhedra are linked by either edge or corner sharing to form infinite chain, sheet, and three-dimensional units. The presence of shared edges allows for cation–cation interactions. Goodenough (1960, 1971), however, has shown that in most of the manganese oxides, these interactions are very weak and that the Mn 3*d*-electrons are essentially localized to their parent cation and its immediate coordination environment. Accordingly, the electronic structures of these minerals should be fairly well approximated by those of simple MnO_6^{n-} clusters.

In this paper, the results of molecular orbital calculations (using the Xα scattered wave method) on such MnO_6 clusters are presented. Calculations were done for MnO_6^{10-}, MnO_6^{9-} and MnO_6^{8-} corresponding to manganese in the 2+, 3+ and 4+ oxidation states, respectively. For all three clusters, octahedral (O_h) symmetry was used. In the structures of manganese oxides, however, the point group symmetries of the MnO_6 clusters are usually much lower (e.g., C_{2v}). Nevertheless, small polyhedral distortions are expected to have only a small effect on orbital energies and charge distributions and the use of O_h symmetry should be a good approximation. Still, calculations on clusters of lower symmetry are desired and will undoubtedly be done as specific examples warrant investigation. For a recent example, Kai et al. (1980) have calculated the electronic structure of MnO_6^{9-} using C_{2v} and D_{4h} symmetry. These results were used to interpret the optical absorption spectrum of Mn^{3+} in andalusite.

In the octahedral clusters investigated here, the Mn^{2+}–O, Mn^{3+}–O and Mn^{4+}–O bond lengths are 2.21Å, 2.04Å and 1.88Å, respectively. These values are representative of those observed in the manganese oxides.

The calculated molecular orbital energies and charge distributions will be used to describe the nature of chemical bonding in manganese oxides. The calculated orbital energies will then be compared with existing spectroscopic data (X-ray emission, ESCA and optical spectra). Finally, the results will be applied to the crystal chemistry of these minerals. In addition to being of direct application to manganese oxide mineralogy, the calculations will also serve to demonstrate the effect of metal atom oxidation state on bonding in coordination sites in minerals.

Theory and method of calculation

The theory behind the Xα scattered wave method has been reviewed in a number of works (Johnson and Smith, 1973; Johnson, 1973; Slater, 1974) and will only be outlined here.

The MnO_6^{n-} cluster is partitioned into a set of overlapping spheres corresponding to the central manganese atom and six oxygen atoms. Within each atomic sphere, the one-electron Schrodinger equation

$$[1/2\nabla^2 + V_c + V_x]\phi_i = \varepsilon_i\phi_i \quad (1)$$

is solved for the orbitals ϕ_i and their energies ε_i. In (1), V_c and V_x are the coulomb and exchange potentials, respectively. These are expressed in terms of the electronic charge density ρ given by

$$\rho = \Sigma(i)n_i\phi_i^*\phi_i \quad (2)$$

where n_i is the occupancy of orbital i. From the charge density the coulomb potential is evaluated using electrostatic theory (solving Poisson's equation) while the exchange potential is evaluated using Slater's Xα approximation

$$V_x = -6\alpha\,[3/4\pi\,\rho]^{1/3} \quad (3)$$

where α is an adjustable scaling factor chosen so that the Xα total energy of the system equals what would be obtained using the conventional Hartree–Fock approach (Schwarz, 1972).

After the individual atomic potentials are calculated to self consistency, they are superimposed to give an initial molecular potential. Within each of the atomic spheres, the new potential is spherically averaged to give a local radial potential. In the interatomic region, the superimposed molecular potential is volume averaged to give a simple constant potential. Finally, a local potential for the extra-molecular region is obtained by spherically averaging the potential within the outer sphere. For each region of the cluster, the Schrodinger equation (using the appropriate potential) is solved. The solutions are then matched at the sphere boundaries using multiple scattered wave theory and the result is then used to derive a new molecular potential. The process is repeated iteratively until a self-consistent result is obtained.

Note that the familiar approximation of molecular orbitals as linear combinations of atomic orbitals (LCAO) is not used. The conceptual utility of this approach is retained in the multiple scattered wave method, however, since the solutions in each region of the cluster are expressed as a summation of functions with definite angular momenta centered at individual atomic sites (partial waves).

A useful feature of the Xα approximation is that the exchange potential (equation 3) for spin up electrons can be different from that for spin down electrons. This is done simply by setting the charge density used in the exchange potential to be only that due to electrons with the same spin. This approach is essential for a realistic treatment of open shell systems (e.g., transition metals with unpaired electrons). If unpaired electrons are present, the exchange potentials, and consequently the spin-up and spin-down orbitals and orbital energies, will be different.

In the conventional Hartree–Fock approach, the energy of a spin-orbital ϕ_i is given by

$$\varepsilon_i = \langle E(n_i - 1)\rangle - \langle E(n_i)\rangle \tag{4}$$

where $\langle E(n_i)\rangle$ is the total energy of the system when the occupancy of orbital ϕ_i is n_i. This is formally known as Koopman's theorem. Note, however, that its derivation assumes that the orbitals remain unchanged during the ionization; this may often be a poor approximation insofar as one expects the orbitals to "relax" about the new electronic configuration of the ionized state. In the Xα formalism, the orbital eigenvalues have a somewhat different meaning: If $\langle E\rangle$ is the total energy of the system, then the orbital eigenvalues ε_i are given by

$$\varepsilon_i = \frac{\partial\langle E(n_i)\rangle}{\partial n_i} \tag{5}$$

Accordingly, the physical nature of the Xα orbital eigenvalues is similar to the notion of "orbital electronegativity".

To evaluate the energy required for a transition from state A to state B, one could calculate the total energy of the system in each state and take the difference. Numerically, this would be very inefficient; electronic transition energies are on the order of a few electron volts while total energies are on the order of 10^4–10^5 electron volts. Slater (1974), however, has shown that one may accurately evaluate the difference between the Xα total energies of two states of a system by using the "transition state" concept. The transition state is defined as having orbital occupancies midway between those found in the initial and final states. Given the transition state configuration, it can be shown that the energy difference between the initial and final states of the system is given by

$$\Delta E = \langle E\rangle_A - \langle E\rangle_B \simeq \sum_i \{n_A(i) - n_B(i)\}\varepsilon_{ts}(i) \tag{6}$$

where $n_A(i)$ and $n_B(i)$ are the occupancies of orbital i in the states A and B, respectively, and $\varepsilon_{ts}(i)$ is the energy of orbital i in the transition state with occupancy

$$n_{ts}(i) = \{n_A(i) + n_B(i)\}/2 \tag{7}$$

One important advantage of the transition state procedure is that it allows one to take into account the orbital relaxation which occurs during the transition.

The essential computational parameters used for the three clusters are given in the appendix. For all clusters, relativistic corrections to the core states were employed.

Calculated molecular orbitals

General

The calculated molecular orbital diagrams of the three clusters are illustrated in Figure 1. Note that the energies of both the spin-up and spin-down forms of each orbital are indicated. The energy levels shown are those of the valence, crystal field, and low energy conduction band molecular orbitals, which in turn are derived from the manganese 3*d*, 4*s*, 4*p* and the oxygen 2*p* atomic orbitals. Each molecular orbital is labelled according to its associated irreducible representation of the O_h point group. The core molecular orbitals (not shown) are essentially the manganese 1*s*, 2*s*, 2*p*, 3*s*, and 3*p* and the oxygen 1*s* atomic orbitals. They are at a much lower energy, do not participate in bonding, and are localized on either the Mn or O atoms. The core states are of interest, however, in the interpretation of X-ray emission and ESCA spectra of Mn-oxides and will be discussed below.

Valence band orbitals

The valence orbitals of t_{1u} symmetry are nominally composed of Mn 4*p* and O 2*p* character. Both the $5t_{1u}$ and $6t_{1u}$ orbitals, however, have essentially no metal atom character, indicating that the Mn 4*p* orbitals are not involved in bonding. The t_{2u} and t_{1g} orbitals are completely non-bonding since they have no symmetry equivalent on the metal atom.

The orbitals of greatest interest are those with both metal and ligand character. These are the valence orbitals of e_g, t_{2g} and a_{1g} symmetry, the atomic compositions of which are given in Table 1. The most important bonding orbitals are the σ-bonding $2e_g$ and the π-bonding $1t_{2g}$. Both of these orbitals are composed of manganese 3*d* and oxygen 2*p* atomic orbitals. With increasing oxidation state of the manganese atom, these orbitals become more bonding in character insofar as they donate more electron density to the Mn atom and become more stable. The spatial nature of these two orbitals can be seen in Figures 2 and 3 which show the wave function contours for the $2e_g$ spin up σ-bonding and $1t_{2g}$ spin up π-bonding molecular orbitals of the MnO_6^{8-} cluster. The σ-bonds (Figs. 2a and 2b) can be pictured as lobes of the Mn $d(x^2 - y^2)$ and $d(3z^2 - r^2)$ atomic orbitals pointing directly at the oxygen *p*-orbitals while the π-bonds (Fig. 3) result from overlap of Mn $d(xy)$, $d(yz)$ and $d(xz)$ orbitals with O *p*-orbitals directed perpendicular to the metal-ligand internuclear vector. The $2e_g$ σ-bonds are strongly directional in character while the $1t_{2g}$ π-bonds are rather delocalized over the three metal-ligand planes. Finally, the σ-bonding $6a_{1g}$ is an important bonding orbital in the MnO_6^{10-} cluster but is of lesser relative importance in the MnO_6^{9-} and MnO_6^{8-} clusters. This orbital is composed of the Mn 4*s* and O 2*p* orbitals.

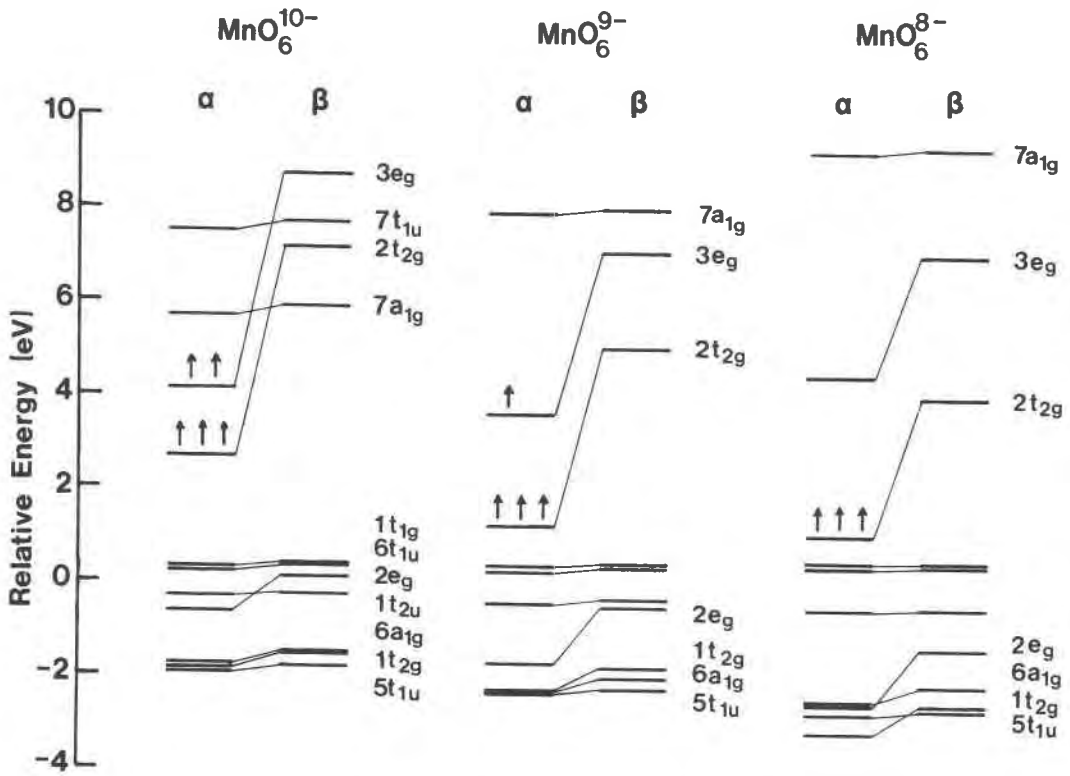

Fig. 1. Molecular orbital diagrams of the three clusters. Orbital energies have been scaled relative to the non-bonding $1t_{1g}$, $1t_{2u}$ and $6t_{1u}$ orbital energies. The number of electrons in the highest occupied molecular orbitals are indicated by the arrow symbols. The α and β symbols indicate spin-up and spin-down orbitals, respectively.

Crystal field orbitals

The $2t_{2g}$ and $3e_g$ orbitals correspond to the one-electron crystal field states. In the pure ionic binding description used by crystal field theory these orbitals are the Mn $3d$ atomic orbitals which have lost their degeneracy by electrostatic interaction with the surrounding anions: the $2t_{2g}$ orbital stabilized by $4Dq$ and the $3e_g$ orbital destabilized by $6Dq$. In the molecular orbital description, the $2t_{2g}$ and $3e_g$ crystal field orbitals are the corresponding anti-

Table 1. Orbital compositions in the three clusters

	MnO_6^{10-}			MnO_6^{9-}			MnO_6^{8-}		
	%Mn	%O	%Int	%Mn	%O	%Int	%Mn	%O	%Int
$3e_g\downarrow$	80	13	6	80	18	1	71	27	2
$3e_g\uparrow$	73	25	1	56	39	4	52	43	4
$2t_{2g}\downarrow$	56	21	23	84	8	8	82	10	8
$2t_{2g}\uparrow$	86	8	6	73	18	8	67	22	10
$2e_g\downarrow$	7	90	2	17	64	17	26	59	13
$2e_g\uparrow$	24	75	1	43	43	13	46	43	10
$1t_{2g}\downarrow$	2	73	24	5	57	36	10	56	33
$1t_{2g}\uparrow$	7	69	23	21	46	32	27	43	29
$6a_{1g}\downarrow$	8	76	16	8	57	34	8	62	30
$6a_{1g}\uparrow$	10	75	15	10	57	33	8	61	29

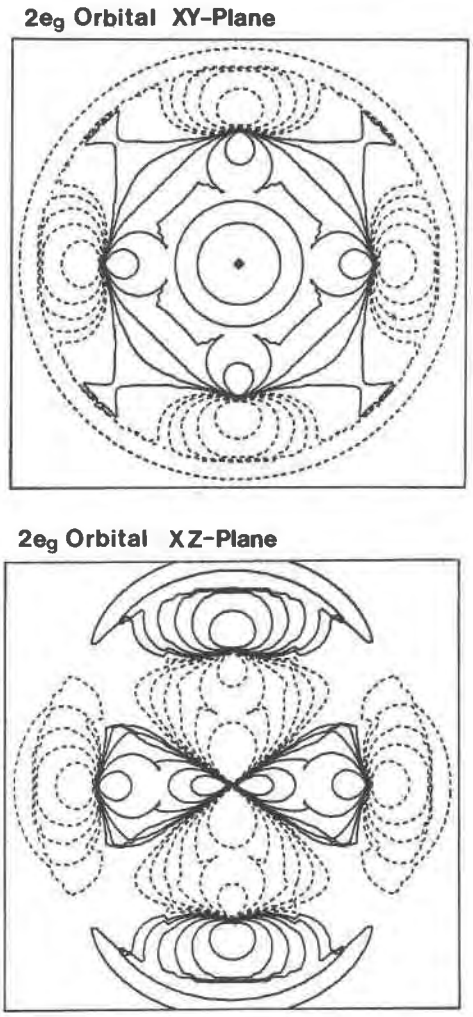

Fig. 2. Wave function contours for the $2e_g$ sigma bonding orbital in the Mn^{4+} centered MnO_6^{8-} cluster. Solid lines indicate the wave function is negative while dashed lines indicate positive values. Contour intervals are given at 0.005, 0.01, 0.02, 0.04, 0.08, and 0.16.

bonding versions of the $1t_{2g}$ and $2e_g$ bonding orbitals. Note that as the metal atom character of the bonding $1t_{2g}$ and $2e_g$ orbitals increases, the ligand character of the antibonding $2t_{2g}$ and $3e_g$ orbitals increases accordingly. Hence, as the $1t_{2g}$ and $2e_g$ orbitals become more bonding in character, the $2t_{2g}$ and $3e_g$ crystal field orbitals become more antibonding. In spite of their antibonding nature, the average energy of the crystal field orbitals, relative to the O $2p$ valence band orbitals, decreases with increasing oxidation state of the manganese atom. Since these orbitals are mostly manganese in character, their increasing stability is a consequence of the increasing electronegativity of the manganese atom. This has important consequences on the ligand to metal charge-transfer spectra of manganese oxides and will be discussed below.

As expected, the crystal field splitting (i.e., the energy separation between the $3e_g$ and $2t_{2g}$ crystal field orbitals) increases with the formal oxidation state of the manganese cation. This is a consequence of two factors: first, an increased electrostatic interaction between the manganese cation and the oxygen anions, and, more importantly, an increased degree of e_g σ-relative to t_{2g} π-bonding in the clusters.

Conduction band orbitals

The energy levels labelled $7a_{1g}$ and $7t_{1u}$ in Figure 1 are those of the lowest energy conduction band orbitals. In the molecular orbital description, these are the σ-antibonding versions of the $6a_{1g}$ and the $5t_{1u}$ bonding orbitals. In an extremely localized or ionic description, these orbitals correspond to the manganese $4s$ and $4p$ atomic orbitals. Their calculated atomic compositions (not given), however, show that they are delocalized over the oxygen, interatomic and extra-molecular regions.

Orbital exchange splittings

As noted previously, when using a spin unrestricted formalism the presence of unpaired electrons will give rise to two different potentials: one for spin up, and one for spin down electrons. In accordance with Hund's rules, electrons with spin up (taken to be the majority spin) are lower in energy than those with spin down. The most extreme case is Mn^{2+} with five unpaired electrons; the resulting energy difference between spin up and spin down states of the partially filled orbitals (the exchange splitting) is quite large. Since the unpaired electrons in each cluster are localized on the metal atom center, the molecular orbitals with the most metal atom character exhibit the greatest exchange splitting.

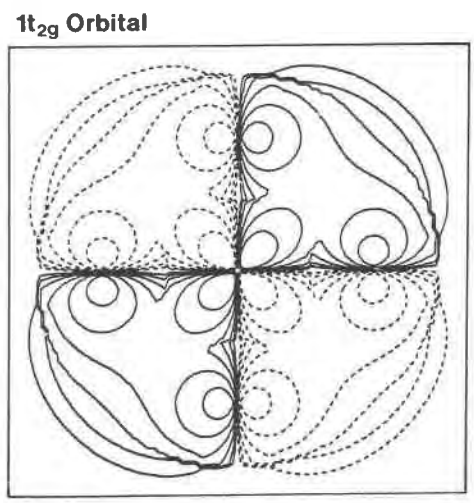

Fig. 3. Wave function contours for the π-bonding spin-up $1t_{2g}$ orbital in MnO_6^{8-}. Contour intervals are as in Fig. 2.

Electronic spectra of manganese oxides

General

The calculated results can be verified by comparing the theoretical orbital energies with existing X-ray emission, ESCA and optical spectra of manganese oxides. The calculated orbital energies can also be used to interpret electronic spectra when band assignments are uncertain.

It is important to recognize, however, that the Xα scattered wave calculations, like all molecular orbital methods, are done using a one-electron formalism. Spectroscopic transitions, however, are between multielectronic wave functions (spectroscopic states). As a consequence of interelectronic repulsion, a given electronic configuration over several one electron orbitals can generate several multielectronic states (see, for example, Lever, 1968). For example, the ground state electronic configuration of Mn^{4+} in MnO_6^{8-} is $(2t_{2g\uparrow})^3$. This configuration gives the multielectronic state $^4A_{2g}$. However, the excited state configuration $(t_{2g\uparrow})^2$ $(e_{g\uparrow})^1$ yields the two states $^4T_{2g}$ and $^4T_{1g}$. Hence, the energy of the one-electron transition $2t_{2g} \rightarrow 3e_g$ corresponds to a weighted average of the energies of the spectroscopic transitions $^4A_{2g} \rightarrow {}^4T_{2g}$ and $^4A_{2g} \rightarrow {}^4T_{1g}$. As a second example, the excited state configuration $(2t_{2g\uparrow})^2(2t_{2g\downarrow})^1$ of MnO_6^{8-} gives the states $^2E_g + {}^2T_{2g} + {}^2T_{1g}$. Hence, the energy of the one-electron transition $2t_{2g\uparrow} \rightarrow 2t_{2g\downarrow}$ corresponds to an average energy for the spin-forbidden spectroscopic transitions $^4A_{2g} \rightarrow {}^2E_g$, $^4A_{2g} \rightarrow {}^2T_{2g}$, and $^4A_{2g} \rightarrow {}^2T_{1g}$. In some cases, an electronic transition between two one-electron orbitals corresponds to a unique transition between two multielectronic spectroscopic states. An example is the $2t_{2g\uparrow}$ to $3e_{g\uparrow}$ transition in MnO_6^{9-}; this corresponds exactly to the $^5E_g \rightarrow {}^5T_{2g}$ spectroscopic transition. Such cases provide an opportunity for direct comparison between calculated and experimental results.

Optical spectra

Transitions between the crystal field orbitals occur in the near-ultraviolet, visible and near-infrared spectral regions. Apart from transitions to higher energy crystal field states, two additional types of transitions occur in the near-ultraviolet: ligand to metal charge transfer and metal to conduction band transitions. Ligand to metal charge-transfer transitions are between the non-bonding ligand orbitals and the metal crystal field orbitals. With reference to the molecular orbitals in Figure 1 these are the $6t_{1u} \rightarrow 2t_{2g}$ and $t_{2u} \rightarrow 2t_{2g}$ transitions. The $1t_{1g} \rightarrow 2t_{2g}$ transition is Laporte forbidden. Metal to conduction band transitions, however, are from the $2t_{2g}$ and $3e_g$ crystal field orbitals (localized on the metal atom) to the $7a_{1g}$ and $7t_{1u}$ conduction band states. Because these transitions may be Laporte allowed, absorption bands are of much greater intensity than those due to crystal field transitions, and often result in an absorption edge in the visible region spectra of transition metal-bearing minerals.

Several investigations have been made of the spectra of Mn^{2+} in oxides and silicates. Pratt and Coelho (1959) obtained the optical spectrum of MnO and estimated values for the ligand field parameters, but these were later revised by the high resolution spectrum of MnO obtained by Huffman et al. (1969). Keester and White (1968) present spectra of Mn^{2+} in a number of minerals. The ground state d^5 electronic configuration gives rise to the ^6S Russel-Saunders term which in turn, gives rise to the $^6A_1$ spectroscopic state in the crystal field. The excited state d-electron configurations which result from promoting a d-electron to one of the spin down d-orbitals, however, give rise to several quartet Russel-Saunders terms. Each of these is split into several states in the crystal field. Hence, a one-electron orbital scheme can provide only the crudest description of the crystal field spectra arising from a high-spin d^5 system. The visible and near-infrared spectrum of Mn^{2+} in octahedral coordination consists of the $^6A_1 \rightarrow {}^4T_1$, $^6A_1 \rightarrow {}^4T_2$ and $^6A_1 \rightarrow {}^4E$, ^4A transitions. The first two transitions are of the set which arise from the $3e_g(\uparrow) \rightarrow 2t_{2g}(\downarrow)$ one-electron transition. The $^6A_1 \rightarrow {}^4E$, $^4A_1$ and higher energy transitions arise from the $2t_{2g}(\uparrow) \rightarrow 2t_{2g}(\downarrow)$ and $3e_g(\uparrow) \rightarrow 3e_g(\downarrow)$ one-electron transitions. In particular, these two "spin-flip" transitions give rise to the quartet states whose energies are independant of $10Dq$ in the Tunabe–Sugano or Orgel diagram for a high-spin d^5 system. One approach to relating the one-electron orbital energies of the MnO_6^{10-} calculation with experimental spectra is to calculate the ligand field parameter $10D_q$. Ligand field theory, however, is cast in a spin-restricted formalism. Hence, a spin-restricted Xα calculation must be done to evaluate ligand field parameters (the correct relation between ligand field theory and the Xα approach is presented by Sambe and Felton, 1976). From such a calculation, the crystal field splitting is found to be 10,900 cm^{-1}; this is in good agreement with the best experimental value of 10,100 cm^{-1} for MnO (Huffman et al., 1969).

Messick et al. (1972) have obtained the near-ultraviolet spectrum of MnO. Transition state calculations were done for the lowest energy absorption features and are compared with the experimental results in Table 2. The calculated results are in good agreement with experimental absorption band energies, yet the band assignments given here are somewhat different. Messick et al. (1972) assigned most of the features between 4.5 and 7.0 eV to transitions from the valence and crystal field bands to the conduction band. Other transitions, based on their temperature dependance, were assigned as metal–metal charge-transfer (i.e., $2Mn^{2+} \rightarrow Mn^+ Mn^{3+}$). No features were assigned as ligand to metal charge-transfer. The calculated results, however, indicate that the first ligand to metal charge-transfer transition is at a very high energy (7.0 eV). At lower energies, but still well into the ultraviolet, are the O $2p$ to conduction band and the metal to conduction band transitions.

Optical absorption spectra are useful for the identifica-

Table 2. Calculated (and observed) optical spectral band energies in manganese oxides

One-Electron Transition	E(calc.)*	Corresponding Spectral Transitions**	References
$(MnO_6)^{8-}$			
$1t_{2u}(\downarrow) \rightarrow 2t_{2g}(\downarrow)$	5.17	$O^{2-} \rightarrow M$ CT	
$6t_{1u}(\downarrow) \rightarrow 2t_{2g}(\downarrow)$	4.32	$O^{2-} \rightarrow M$ CT (ca. 4.3)	1
$2t_{2g}(\downarrow) \rightarrow 3e_g(\downarrow)$	3.33	$^4A_2 \rightarrow {}^4T_2$ (2.64), $^4T_1$	1
$2t_{2g}(\downarrow) \rightarrow 2t_{2g}(\downarrow)$	2.95	$^4A_2 \rightarrow {}^2E$, $^2T_1$, $^2T_2$	
$(MnO_6)^{9-}$			
$1t_{2u}(\downarrow) \rightarrow 2t_{2g}(\downarrow)$	6.27	$O^{2-} \rightarrow M$ CT	
$6t_{1u}(\downarrow) \rightarrow 2t_{2g}(\downarrow)$	5.55	$O^{2-} \rightarrow M$ CT	
$6t_{1u}(\downarrow) \rightarrow 3e_g(\downarrow)$	4.65	$O^{2-} \rightarrow M$ CT (4.09,4.2,4.5)	2
$2t_{2g}(\downarrow) \rightarrow 3e_g(\downarrow)$	2.42	$^5E \rightarrow {}^5T_2$ (2.25-2.73)	3,4,5
$2t_{2g}(\downarrow) \rightarrow 2t_{2g}(\downarrow)$	3.42		
$(MnO_6)^{10-}$			
$6t_{1u}(\downarrow) \rightarrow 2t_{2g}(\downarrow)$	7.00	$O^{2-} \rightarrow M$ CT (7.2, 6.9)	6
$1t_{1g}(\downarrow) \rightarrow 7t_{1u}(\downarrow)$	5.80	VB $\rightarrow$ CB (5.7)	6
$2t_{2g}(\downarrow) \rightarrow 7t_{1u}(\downarrow)$	5.17	CF $\rightarrow$ CB (5.4?)	6

*Energies in eV (1 eV = 8.066 × 10^3 cm^{-1}). **Observed spectral features given in parentheses. References: 1. Geschwind et al.(1962); 2. Langer and Abu-Eid (1979); 3. Burns and Strens (1967); 4. Burns (1970); 5. Halenius (1978); 6. Messick et al. (1972).

tion of Mn^{3+} cations in oxides and silicates (Burns, 1970). The calculated energy for the $^5E_g \rightarrow {}^5T_{2g}$ crystal field transition in the MnO_6^{9-} cluster is 19,520 cm^{-1}. This also corresponds to the $10D_q$ parameter of ligand field theory. In most Mn^{3+}-bearing minerals the local coordination environment is distorted to tetragonal (D_{4h}) symmetry by the Jahn–Teller effect. There has been some confusion as to the definition of $10D_q$ in non-cubic symmetries and hence the $10D_q$ values reported for Mn^{3+} in epidote (Burns and Strens, 1967), manganophyllite (Burns, 1970) and andalusite (Halenius, 1978; Kai et al., 1980) do not correspond to the cubic crystal field value of $10D_q$. In D_{4h} symmetry, the cubic crystal field parameter $10D_q$ corresponds to the $^5B_{1g} \rightarrow {}^5B_{2g}$ spectroscopic transition energy (see, for example, Konig and Kremer, 1977). From the spectra of Mn^{3+} in epidote (Burns and Strens, 1967), manganophyllite (Burns, 1970) and andalusite (Halenius, 1978) the cubic $10D_q$ values are therefore found to be 18,170 cm^{-1}, 19,050 cm^{-1} and 22,000 cm^{-1}, respectively. Hence, the value calculated for the MnO_6^{9-} cluster is reasonable. McClure (1962), however, has obtained a $10Dq$ value of 19,470 cm^{-1} for Mn^{3+} in corundum; since the Mn^{3+}–O bond length in this phase is expected to be much shorter than the 2.04Å used in this calculation, it appears that the value of $10D_q$ obtained here may be too high. On the other hand, the $10D_q$ value of the Mn^{3+} aquocomplex is 21,000 cm^{-1} (Orgel, 1966).

The only near-ultraviolet spectral data for Mn^{3+} in minerals, from which one may obtain ligand-to-metal charge-transfer energies, is the spectrum of piemontite obtained by Langer and Abu-Eid (1977). Strong bands were observed at 33,000 and 34,000 cm^{-1}. These may be assigned to the $6t_{1u} \rightarrow 3e_g$ transition which is calculated to be at 4.6 eV (37,000 cm^{-1}) in the MnO_6^{9-} cluster. Calculated values for other spectral band energies are given in Table 2.

The spectrum of Mn^{4+} in corundum has been obtained by Geschwind et al. (1962). As noted previously, the one-electron orbital transition $2t_{2g}(\uparrow) \rightarrow 3e_g(\uparrow)$ in MnO_6^{8-} corresponds to the two spectroscopic transitions $^4A_2 \rightarrow {}^4T_2$ and $^4A_2 \rightarrow {}^4T_1$. In the spectrum of Mn^{4+} in corundum, however, only the $^4A_2 \rightarrow {}^4T_2$ transition was observed and its energy was 21,300 cm^{-1}. The energy calculated for the one-electron orbital transition $2t_{2g} \rightarrow 3e_g$ is 26,860 cm^{-1}. Since this corresponds to an average of the two spectroscopic transition energies, it is in qualitative agreement with experiment. Finally, the energy of the first ligand to metal charge-transfer transition was estimated to be about 35,000 cm^{-1}. This agrees with the calculated value of 34,850 cm^{-1} for the $6t_{1u} \rightarrow 2t_{2g}$ ligand to metal charge transfer transition. The calculated energies for the remaining ligand to metal charge-transfer and crystal field orbital transitions of MnO_6^{8-} are given in Table 2.

The energies of the ligand to metal charge-transfer and metal to conduction band transitions in the three clusters correlate with the relative oxidation and reduction poten-

tials of the three valences of manganese (e.g., Huheey, 1978). In the MnO_6^{10-} cluster, the first metal to conduction band transition is much lower in energy than the first ligand to metal charge-transfer transition; likewise the oxidation of Mn^{2+} to Mn^{3+} requires less energy than the reduction of Mn^{2+} to Mn^{+}. In the MnO_6^{8-} cluster however, the first ligand to metal charge transfer transitions are much lower in energy than the first metal to conduction band transitions; likewise the reduction of Mn^{4+} to Mn^{3+} is more energetically favorable than the oxidation of Mn^{4+} to Mn^{5+}. An intermediate situation is provided by MnO_6^{9-} where the two types of transitions are of similar energies.

X-ray emission spectra

When an electron from a 1*s* core orbital has been photoejected, transitions from the higher energy occupied orbitals to the 1*s* orbital occur. The emitted photons accompanying the relaxation give rise to the *K* spectrum. For first row transition metals, the transitions of greatest interest are those that originate from the n = 3 atomic orbitals (*M*-shell) since these are strongly influenced by the oxidation state and local coordination environment of the metal atom. The transitions of the type $3p_{3/2}$, $3p_{1/2}$, 3*d* etc. $\rightarrow$ 1*s* define the $K\beta$ spectrum. The main peak in the $K\beta$ spectrum results from the Mn 3*p* $\rightarrow$ Mn 1*s* transition and is designated $K\beta_1$. In addition to the $K\beta_1$ transition, several addition peaks are observed. The $K\beta_5$ peak is due to transitions which are nominally of the type Mn 3*d*, O 2*p* $\rightarrow$ Mn 1*s*. The satellite lines $K\beta''$ and $K\beta'''$ are attributed to O 2*s* $\rightarrow$ Mn 1*s* and Mn 4*p* (conduction band) $\rightarrow$ Mn 1*s* transitions, respectively. By analogy with the *K* spectrum, the *L* spectrum results from transitions to the n = 2 atomic levels (i.e., 2*s* and 2*p* levels). The 2*p* level is split by spin-orbit coupling into the $2p_{1/2}$ and $2p_{3/2}$ states. Hence, in first-row transition metals, two allowed transitions are present: $3d \rightarrow 2p_{1/2}$ ($L\beta_1$) and $3d \rightarrow 2p_{3/2}$ ($L\alpha_{1,2}$).

The $K\beta$ and $L\alpha$, $L\beta$ spectra of MnO and MnO_2 were calculated using the transition state formalism. These results are presented in Table 3 and compared with experimental values (Koster and Mendel, 1970; Tsutsumi et al., 1976; Wood and Urch, 1976). The agreement between theory and experiment is good for the case of MnO although the $K\beta$ energies may be overestimated for the case of MnO_2. The results can also be used to interpret the $K\beta$ spectra of MnO, Mn_2O_3 and MnO_2 phases. The assignment of $K\beta''$ (Koster and Mendel, 1970) or "peak A" (Tsutsumi et al., 1976) to the O 2*s* $\rightarrow$ Mn 1s crossover transition seems to be correct. Similarly, the assignment of $K\beta'''$ to a transition of an excited electron in the Mn 4*p* ($7t_{1u}$) orbital to the Mn 1*s* orbital (Koster and Mendel, 1970) seems reasonable. An additional satellite peak, labeled $K\beta'$, was attributed by Koster and Mendel (1970) to a discrete energy loss process whereby a $K\beta_1$ photon excites a Mn 3*d* electron into the $7t_{1u}$ conduction band. Based on the ground state energies, this does not appear to be correct. Tsutsumi et al. (1976) attribute this feature to exchange splitting of the $K\beta_1$ peak.

X-ray photoelectron spectra (ESCA)

Valence region photoelectron spectra of MnO, Mn_2O_3 and Mn_3O_4 have been investigated. A low resolution spectral profile encompassing the Mn 3*d*, O 2*p* and O 2*s* valence bands of MnO (Wertheim and Hufner, 1972; Hufner and Wertheim, 1973) showed that the O 2*p* and O 2*s* bands are separated by their free ion value of ~16 eV; this is in agreement with the results obtained here (i.e., the $1t_{1g}$, $6t_{1u}$ (2*p*) $-$ $1e_g$, t_{1u}, a_{1g} (2*s*) energy separations). Rao et al. (1979) have obtained fairly high resolution spectra profiling the O 2*p* and Mn 3*d* bands in MnO, Mn_2O_3 and Mn_3O_4. In the spectra of both MnO and Mn_2O_3, four peaks were observed and were assigned to be the Mn 3*d* (e_g), Mn 3*d* (t_{2g}), O 2*p* (σ) and O 2*p* (π) bands. The peaks were separated by about 1.5–2.0 eV and, accordingly, are in fairly nice agreement with the ground state energy level diagrams presented in Figure 1. In the spectrum of the mixed-valence phase hausmannite (Mn_3O_4), they were able to easily resolve the Mn^{2+} and Mn^{3+} 3*d*-bands. These states were found to have the energetic order Mn^{2+} (e_g) > Mn^{3+} (e_g) > Mn^{2+} (t_{2g}) > Mn^{3+} (t_{2g}). This ordering is in agreement with the ground

Table 3. Calculated and experimental *K* and *L* spectra of MnO and MnO_2

		MnO		MnO_2		
Band	Transition	E (exp)	E (calc)	E (exp)	E (calc	Ref
$K\beta_1$	Mn 3p → 1s	6491.8	6495.1	6490.0	6495.1	1,2
Kβ''	O 2s → 1s	~6521.0	6520.0	6521.0	6528.5	1
$K\beta_5$	$5t_{1u}$ → 1s	6533.2	6532.8	6534.7	6541.0	1,2,3
Kβ'''	$7t_{1u}$ → 1s	~6549.8	6549.5	6549.8		1
Lα	$2t_{2g}$ → 2p	643.	643.1	643.	643.3	3

1. Koster and Mendel (1970); 2. Tsutsumi et al. (1976); 3. Wood and Urch (1976).

state electronic structures of the isolated MnO_6^{10-} and MnO_6^{9-} clusters if their orbital energies are related by setting the intersphere potentials to be equal (as in Fig. 1).

Applications to the crystal chemistry of manganese oxides

Molecular orbital calculations on finite clusters can be used to assess the stability of a given cation valence state and electronic configuration (e.g., high-spin vs. low-spin) in a given coordination environment. Ideally, this information can then be applied to understanding mineral stabilities, cation site occupancies, and the speciation and transport of transition metals in geochemical environments.

Chemical bonding in manganese oxides

Of fundamental importance is the relative ionic versus covalent nature of the manganese–oxygen bond. Of additional interest is the exact nature of the covalent interaction. In each of the clusters, electronic charge is donated from the O^{2-} anions to the Mn^{2+}, Mn^{3+} or Mn^{4+} cations. One way to describe the nature of the manganese–oxygen bond in each cluster is to calculate the net amount of electronic charge donated to the manganese center by each of the different types of metal-ligand bonding interactions. For each orbital, however, the relative amount of electronic charge in the atomic versus interatomic regions is a function of the atomic sphere radii used in the calculation. To eliminate the dependance of the bonding description on the sphere radii, it is necessary to partition the intersphere electronic charge among the manganese and oxygen atomic regions. A reasonable way of doing this is according to the ratio of manganese to oxygen atomic sphere charges. This was done for each orbital and the calculated net amount of electronic charge donated to the manganese center by the different types of orbital interactions is presented in Table 4.

By summing the amount of electronic charge donated by each type of orbital interaction, one may calculate a relative degree of covalancy of the bonding in each cluster. The calculations show that the bonding in manganese(IV) oxides is mostly covalent. The strong covalency of the Mn^{4+}–O bond is also in agreement with the strong Lewis acidity of Mn^{4+} in aqueous environments. In contrast, the bonding in the Mn^{2+} cluster is mostly ionic; this is in agreement with the tendency for Mn^{2+} to act as a weak Lewis acid and as an exchangable cation in sedimentary environments.

Table 4. Net electronic charge donated to the manganese cations by each type of orbital.

	MnO_6^{10-}	MnO_6^{9-}	MnO_6^{8-}
$e_g(\sigma)$	-0.124	-0.986	-1.624
$t_{2g}(\pi)$	-0.096	-0.549	-0.831
$a_{1g}(\sigma)$	-0.213	-0.271	-0.228
$t_{1u}(\sigma)$	-0.156	-0.272	-0.261
$\sum q =$	-0.589	-2.078	-2.945
% Covalency	29.5	69.3	73.6

It can be seen that in the Mn^{3+} and Mn^{4+} clusters most of the metal-ligand interaction is through the e_g σ-type bonds (Mn 3*d*–O 2*p* overlap). There is also an appreciable degree of π-type bonding interaction as well. Since the former bond type is quite directional in character, it is expected that the stabilities of these cations in oxides should have a strong dependence on coordination site geometry. Molecular orbital calculations on MnO_6^{9-} and MnO_6^{8-} clusters using different site geometries might therefore be of interest. In contrast, most of the metal-ligand interaction in the MnO_6^{10-} cluster results from the spherically symmetric a_{1g} σ-type interaction and the spatially diffuse t_{1u} interaction. This situation, together with the fairly ionic nature of the Mn^{2+}–O bond, suggests that the stability of a Mn^{2+} cations should exhibit a weaker dependence on its coordination geometry.

Octahedral versus tetrahedral coordination

In the crystal structures of the manganese(IV) oxides, the Mu^{4+} cations are only in octahedral coordination (Burns and Burns, 1977; 1979). The ionic radius of Mn^{4+} (Shannon and Prewitt, 1969), however, is less than or equal to that of several cations which often occur in tetrahedral coordination (e.g., Al^{3+}, Fe^{3+}, and even Mn^{2+}). Crystal field theory explains the greater stability of octahedrally coordinated Mn^{4+} since a d^3 transition metal cation will have an octahedral site preference energy of $38/45\Delta_{oct}$ (where Δ is the crystal field splitting and it is assumed that $\Delta_{tet} = 4/9\Delta_{oct}$). Given the calculated crystal field splitting of the *d*-orbitals in the MnO_6^{8-} cluster, the octahedral site preference energy is found to be 2.79 eV. This is an extremely large value and it accounts well for the absence of tetrahedrally coordinated Mn^{4+} in minerals.

Although crystal field theory has been quite successful when applied to the crystal chemistry of the transition metals (Burns, 1970), its physical basis is unfounded. A more physically correct approach is molecular orbital theory. To apply molecular orbital theory to understanding the stability of octahedrally coordinated Mn^{4+} in oxide minerals, a calculation was done for a tetrahedral MnO_4^{4-} cluster. The bond length is taken to be the sum of the Shannon and Prewitt (1969) ionic radii for fourfold-coordinated Mn^{4+} and twofold-coordinated O^{2-}. The resulting molecular orbital diagram is compared with that of the octahedral MnO_6^{8-} cluster in Figure 4. In the molecular orbital formalism, the notion of octahedral site preference energy is somewhat complicated; still, several differences between the two clusters are apparent. Relative to the top of the oxygen 2*p* valence band (the t_1

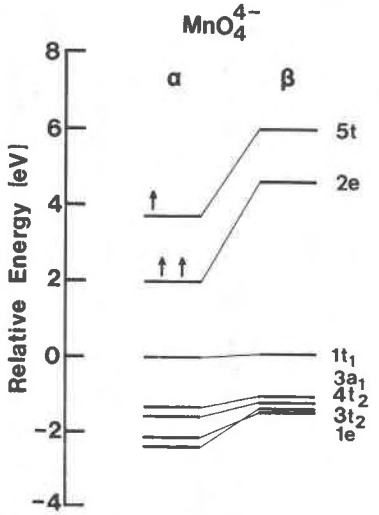

Fig. 4. Molecular orbital diagram for tetrahedral MnO_4^{4-}(R = 1.74Å).

orbital in T_d symmetry and the t_{1g} orbital in O_h symmetry), the occupied Mn^{4+} crystal field orbitals are less stable in the tetrahedral cluster. Moreover, in T_d symmetry one electron must occupy the least stable $5t_2$ orbital which is σ-antibonding. Finally, the bonding molecular orbitals in the MnO_6^{8-} cluster are more stable (by about 1 eV) than the analogous orbitals in the MnO_4^{4-} cluster. This is probably due to an increased delocalization of the valence orbital electrons in the larger MnO_6^{8-} cluster. The molecular orbital approach shows that Mn^{4+} is more stable in octahedral coordination although it is somewhat ambiguous as to how one may define an octahedral site preference energy.

High- versus Low-spin Mn^{2+} and Mn^{3+}

Transition metals with more than three electrons can exist in both high spin and low spin states in octahedral coordination. The two spin states of a transition metal cation have different ionic radii (Shannon and Prewitt, 1969) and, hence, different crystal-chemical behavior. The spin-unrestricted calculations can provide insight into the stability of the high-spin relative to the low-spin configuration in a given coordination environment. As noted previously, the calculations show that both Mn^{2+} and Mn^{3+} are in high-spin configurations at the metal-ligand bond distance used for the MnO_6^{10-} and MnO_6^{9-} clusters. The exchange splitting of the Mn^{2+} crystal field orbitals (Fig. 1) is quite large (4.5 eV); this indicates that the high-spin configuration $t_{2g}\ (\uparrow)^3 e_g(\uparrow)^2$ of Mn^{2+} is much more stable than the low-spin configuration $t_{2g}(\uparrow)^3 t_{2g}(\downarrow)^2$. It is known that with increasing pressure transition metals may undergo a high spin to low-spin transition. Such a transition of Fe^{2+} is inferred to occur in the Earth's mantle (Fyfe, 1960; Strens, 1969; Burns, 1970). The electronic structure of the MnO_6^{10-} cluster, however, implies that a high-spin to low-spin transition of Mn^{2+} is unlikely, and that Mn^{2+} in the Earth's mantle is in the high-spin state.

In contrast, the smaller exchange splitting of the $2t_{2g}$ orbital and the larger crystal field splitting in the MnO_6^{9-} cluster suggest that a high-spin to low-spin transition of Mn^{3+} can occur. When the Mn–O distance in the MnO_6^{9-} cluster is decreased from 2.04 to 1.88Å, the low-spin configuration is found to be the most stable; this suggests that low-spin Mn^{3+} may substitute for Mn^{4+} in the manganese(IV) oxides, the ionic radii of Mn^{4+} and low-spin Mn^{3+} being fairly similar (Shannon and Prewitt, 1969). It should be noted, however, that Mn^{3+} distorts its coordination environment via the Jahn–Teller effect and that the resulting tetragonal distortion will stabilize the high-spin configuration. Spin-unrestricted calculations on MnO_6^{9-} clusters with D_{4h} symmetry should therefore be done to investigate this problem.

Stability of Mn^{3+} cations in oxides

The Mn^{3+} ion is often unstable and frequently disproportionates to Mn^{2+} and Mn^{3+} ions (Stumm and Morgan, 1970; Huheey, 1978; Cotton and Wilkinson, 1980). The molecular orbital diagrams in Figure 1 suggest that the stability of the MnO_6^{9-} cluster is approximately midway between that of the MnO_6^{10-} and MnO_6^{7-} clusters. Hence, in oxides, the energy required for the disproportionation of two Mn^{3+} ions should be quite low. Following Tossell (1978), one may perform a transition state calculation for the disproportionation of two MnO_6^{9-} clusters to a MnO_6^{8-} and a MnO_6^{10-} cluster as follows: 0.5 electrons are removed from the $3e_g$ orbital of the MnO_6^{10-} cluster and added to the $3e_g$ orbital of the MnO_6^{8-} cluster. The orbital energies of the two isolated clusters can be placed on the same scale by equating their constant intersphere potentials. The resulting energy difference between the MnO_6^{8-} and MnO_6^{10-} $3e_g$ orbitals would correspond to the energy required for the disproportionation. This is found to be less than 0.25 eV. This approach, however, neglects the electrostatic component of the cluster energies. Moreover, the Mn^{3+} cation will stabilize itself by inducing a tetragonal distortion of its coordination environment. Still, the calculations seem to be qualitatively consistent with the known chemical behavior of Mn^{3+} and suggest that one may relate trends in redox chemistry with theoretical valence orbital energies.

Conclusions

The agreement between the calculated results and experimental spectra of manganese oxides demonstrates that isolated clusters can be used to model chemical bonding in these minerals.

As the formal oxidation state of the manganese atom increases, the Mn–O bond becomes more covalent, the crystal field splitting increases and the exchange splitting of the *d*-orbitals decreases. The covalent nature of the bonding in the MnO_6^{8-} cluster explains the low solubilities

of manganese (IV) oxides in solutions where strong complexing agents are absent. In contrast, the ionic nature of the bonding in the MnO_6^{10-} cluster is in agreement with the higher solubility of Mn^{2+} in aqueous solutions and the ability of Mn^{2+} to act as an exchangeable cation in complex oxides.

In terms of crystal field theory, the large crystal field splitting in the MnO_6^{8-} cluster explains the absence of tetrahedrally coordinated Mn^{4+} in minerals. In terms of molecular orbital theory, a comparison of the calculated electronic structures of octahedral MnO_6^{8-} and tetrahedral MnO_6^{4-} clusters indicates that Mn^{4+} is much less stable in tetrahedral coordination.

Because the bonding in the MnO_6^{10-} cluster is mostly ionic, the Mn^{2+} 3*d*-orbital electrons are strongly localized on the metal atom. Since there are five unpaired electrons, this gives rise to a large exchange splitting of the crystal field orbitals. This, in turn, indicates that a high-spin to low-spin transition of Mn^{2+} in oxides and silicates at high pressure is unlikely.

Finally, the calculations are in qualitative agreement with the tendency for Mn^{3+} cations to disproportionate. In addition, it is found that at the Mn–O bond distances found in the manganese (IV) oxides, Mn^{3+} would be in a low-spin configuration. This suggests that low-spin Mn^{3+} may substitute for Mn^{4+} in manganese oxides.

Acknowledgments

I am especially grateful to Jack Tossell, Dept. of Chemistry, University of Maryland, for initial guidance and encouragement. I would also like to thank Roger Burns, Keith Johnson and Paco Leon for many helpful discussions. This work was supported by NASA grant NSG-7604 and NSF grant No. EAR 80-16163 to Roger Burns.

References

Burns, R. G. (1970) Mineralogical Applications of Crystal Field Theory. Cambridge University Press, London.

Burns, R. G. and Burns, V. M. (1979) Manganese oxides. In R. G. Burns, Ed., Marine Minerals, Reviews in Mineralogy, Vol. 6, p. 1–46. Mineralogical Society of America, Washington, D.C.

Burns, R. G. and Burns, V. M. (1977) Mineralogy of manganese nodules. In G. P. Glasby, Ed., Marine Manganese Deposits, p. 185–248. Elsevier, New York.

Burns, R. G. and Strens, R. G. J. (1967) Structural interpretation of the polarized absorption spectra of Al–Fe–Mn–Cr epidotes. Mineralogical Magazine, 36, 204–206.

Cotton, F. A. and Wilkinson, G. (1980) Advanced Inorganic Chemistry, 4th edition. John Wiley and Sons, New York.

Fyfe, W. S. (1960) The possibility of *d*-electron coupling in olivine at high pressure. Geochimica et Cosmochimica Acta, 19, 141–143.

Geschwind, S., Kislink, P., Klein, M. P., Remeika, J. P., and D. L. Wood (1962) Sharp-line fluorescence, electron paramagnetic resonance and thermoluminescence of Mn^{4+} in αAl_2O_3. Physical Review, 126, 1684–1686.

Goodenough, J. B. (1960) Direct cation–cation interactions in several oxides. Physical Review, 117, 1442–1451.

Goodenough, J. B. (1971) Metallic oxides. Progress in Solid State Chemistry, 5, 145–399.

Halenius, U. (1978) A spectroscopic investigation of manganian andalusite. Canadian Mineralogist, 16, 567–575.

Huffman, D. R., Wild, R. L., and Shinmei, M. (1969) Optical absorption spectra of crystal field transition in MnO. The Journal of Chemical Physics, 50, 4092–4094.

Hufner, S. and Wertheim, G. K. (1973) X-ray photoelectron band structure of some transition metal compounds. Physical Review B, 8, 4857–4867.

Huheey, J. E. (1978) Inorganic Chemistry, 2nd edition. Harper and Row, New York.

Johnson, K. H. (1973) Scattered wave theory of the chemical bond. Advances in Quantum Chemistry, 7, 143–185.

Johnson, K. H. and Smith, F. C. (1972) Chemical bonding of a molecular transition metal ion in a crystalline environment. Physical Review B, 5, 831–843.

Kai, A. T., Larsson, S., and Halenius, U. (1980) The electronic structure and absorption spectrum of MnO_6^{9-} octahedra in manganoan andalusite. Physics and Chemistry of Minerals, 6, 77–84.

Keester, A. S. and White, W. B. (1968) Crystal field spectra and chemical bonding in manganese minerals. In Papers and Proceedings of the Fifth General Meeting, International Mineralogical Association, 1966, p. 22–35. Mineralogical Society, London.

Konig, E. and Kremer, S. (1977) Ligand Field Energy Diagrams. Plenum Press, New York.

Koster, A. S. and Mendel, H. (1970) X-ray K emission spectra and energy levels of compounds of 3d-transition metals-I oxides. Journal of Physics and Chemistry of Solids, 31, 2511–2522.

Langer, K. and Abu-Eid, R. M. (1977) Measurement of the polarized absorption spectra of synthetic transitio metal-bearing microcrystals in the spectral range 44,000-4,000 cm^{-1} Physics and Chemistry of Minerals, 1, 273–299.

Lever, A. P. B. (1968) Inorganic Electron Spectroscopy. Elsevier, Amsterdam.

McClure, D. S. (1962) Optical spectra of transition metal ions in corundum. Journal of Chemical Physics, 36, 2757–2779.

Messick, L., Walker, W. C., and Glosser, R. (1972) Direct and temperature modulated reflectance spectra of MnO, CoO and NiO. Physical Review B, 6, 3941–3949.

Norman, J. G. (1976) Non-empirical versus empirical choices for overlapping sphere radii rations in SCF-Xα-SW calculations on ClO_4^- and SO_2. Molecular Physics, 31, 1191–1198.

Pratt, G. W. J. and Coehlo, R. (1959) Optical absorption of CoO and MnO above and below the Neel temperature. Physical Review, 116, 281–286.

Rao, C. N. R., Sarma, D. D., Vasidevan, S., and Hegde, M. S. (1979) Study of transition metal oxides by photoelectron spectroscopy. Proceedings of the Royal Society of London A, 367, 239–252.

Sambe H. and Felton, R. H. (1976) Connection between the Xα method and ligand field theory. International Journal of Quantum Chemistry Symposium, 10, 155–158.

Schwarz, K. (1972) Optimization of the statistical exchange parameter α for the free atoms H through Nb. Physical Review B, 5, 2466–2468.

Shannon, R. D. and Prewitt, C. T. (1969) Effective ionic radii in oxides and fluorides. Acta Crystallographica, B25, 925–946.

Slater, J. C. (1974) The Self Consistent Field Method for Atoms, Molecules and Solids: Quantum Theory of Molecules and Solids, Volume 4. McGraw Hill, New York.

Strens, R. G. J. (1969) The nature and geophysical importance of spin pairing in minerals of iron (II). In The Application of Modern Physics to the Earth and Planetary Interiors. Wiley-Interscience, London.

Stumm, W. and Morgan, J. J. (1970) Aquatic Chemistry. John Wiley and Sons, New York.

Tossell, J. A. (1978) Theoretical studies of the electronic structure of copper in tetrahedral and triangular coordination with sulfur. Physics and Chemistry of Minerals, 2, 225–236.

Tossell, J. A., Vaughan, D. J., and Johnson, K. H. (1974) The electronic structure of rutile, wustite and hematite from molecular orbital calculations. American Mineralogist, 59, 319–334.

Tossell, J. A. and Gibbs, G. V. (1977) Molecular orbital studies of geometry and spectra of minerals and inorganic compounds. Physics and Chemistry of Minerals, 2, 21–57.

Tsutsumi, K., Nakamori, H., and Ichikawa, S. K. (1976) X-ray Mn K emission spectra of manganese oxides and manganates. Physical Review B, 13, 929–933.

Wertheim, G. K. and Hufner, S. (1972) X-ray photoemission band structure of some transition metal oxides. Physical Review Letters, 28, 1028–1031.

Wood, P. R. and Urch, D. S. (1976) Valence band x-ray emission spectra of manganese in various oxidation states. Journal of the Chemical Society, Dalton Transactions, 2472–2476.

Manuscript received, April 12, 1983;
accepted for publication, January 9, 1984.

Appendix

For the MnO_6^{10-} calculation, sphere radii were chosen using the procedure of Norman (1977). Mn, O, and outer sphere radii used were 2,4266, 2.5919, and 6.7681 bohrs, respectively. This choice of radii gave a virial theorem coefficient of 1.006.

For the MnO_6^{9-} and MnO_6^{8-} calculations sphere radii were chosen using the above procedure but without taking into account the Watson spheres surrounding the oxygen atoms. The Mn, O and outer sphere radii used in the MnO_6^{9-} calculation were 2.2580, 1.7099 and 5.5656 bohrs, respectively. This choice gave a virial theorem coefficient of 1.008. The Mn, O and outer sphere radii used in the MnO_6^{8-} cluster were 2.0790, 1.7080 and 5.2610 bohrs, respectively. The resulting virial theorem coefficient was 1.008.

In each cluster, partial waves up to $l = 2$ were used for manganese, $l = 1$ were used for oxygen, and $l = 4$ were used for the Outer sphere.